Scientific Research and Essays

Academic Journals

ABOUT SRE

The **Scientific Research and Essays (SRE)** is published twice monthly (one volume per year) by Academic Journals.

Scientific Research and Essays (SRE) is an open access journal with the objective of publishing quality research articles in science, medicine, agriculture and engineering such as Nanotechnology, Climate Change and Global Warming, Air Pollution Management and Electronics etc. All papers published by SRE are blind peer reviewed.

Contact Us

Editorial Office: sre@academicjournals.org

Help Desk: helpdesk@academicjournals.org

Website: http://www.academicjournals.org/journal/SRE

Submit manuscript online   http://ms.academicjournals.me/.

Scientific Research and Essays

<u>ARTICLE</u>

Scientific Research and Essays

Full Length Research Paper

Strain field determination using displacement gradient model and unified least-squares technique

Yi-Chun Lin* and Jen-Yu Han

Department of Civil Engineering, National Taiwan University, Taipei 10617, Taiwan.

Deformation analysis is crucial to applications in geodesy, structural engineering, and geology, of which the main goal is to detect the behaviors of a deformed body. Traditional deformation analyses rely on a limited number of observations and thus give a relatively poor description of the strain field on the entire object. In this study, a method based on the displacement gradient model and unified least-squares adjustment is proposed to improve classical deformation analysis. Corresponding quality assessment and sensitivity analysis are derived accordingly to better assess significant deformation. Furthermore, by applying nearest neighbor searching and a triangulated irregular network, the efficiency of analyzing a vast number of observations is improved. Numerical experiments based on real data suggested that the proposed approach detected behaviors of a deformed body in an effective and efficient way. Consequently, the strain field on an object can be obtained rapidly and accurately using the proposed method and a large point dataset.

Key words: Deformation analysis, strain field, dispersed point data, structural health monitoring.

INTRODUCTION

In civil engineering, deformation analysis is fundamental to understanding the mechanical properties and failure mechanisms of an object. Deformation, the change in shape of an object subjected to force, is quantified by the normalized measurement "strain". Traditional deformation measurement is collected by strain gauges (contact sensors) or total stations (noncontact sensors). However, these techniques can only obtain a small number of observations with constraints in hardware installation (for contact sensors) and time-consuming field works. Even with a robotic total station, the number of observations is

still limited by the manually-observed process. As a result, traditional measuring techniques are impractical for capturing the displacement field and strain field. Digital image correlation (DIC) and Light Detection and Ranging (LiDAR) are two modern techniques which can automatically obtain massive and high quality spatial data in an efficient way. Both the techniques can provide data with an accuracy sufficient for not only large-scale change detection, but also small deformation monitoring (Chu et al., 1985; Gonzalez-Jorge et al., 2011, 2012; Park et al., 2007). In digital image processing field, many

*Corresponding author. E-mail: slps9060622@gmail.com. Tel: +886-2-33664347.

image-based methods have been introduced to estimate the displacement field and strain field on an object (Aydilek et al., 2004; Lee et al., 2011; Pan et al., 2009, 2015; Winkler et al., 2014). LiDAR have also been further developed and applied to perform deformation analysis in various fields (e.g. structural health monitoring, Lee and Park, 2011; shape modelling, Armesto et al., 2010; cultural heritage conservation, Pesci et al., 2011; rockfall monitoring, Alba and Scaioni, 2010).

The most important part of deformation analysis is to establish a mathematical model. A good mathematical model extracts deformation signals from raw data, which usually contain rigid body motion and variation of the reference frame (Vaníček et al., 2008; Han et al., 2009). The displacement model and the affine model are two typical mathematical models. The two models are based on distinct theories and have different assumptions. The displacement model assumes that the deformation at any initial point of an object is affected by several neighboring points, and thus the deformation at the initial point can be solved by integrating the displacement vectors of the neighboring points (Vaníček et al., 2001, 2008; Berber et al., 2006; Marjetič et al., 2009). On the other hand, the affine model assumes the deformation to be homogeneous in the whole study area, and thus it can be symbolized by the same parameters (Mikhail et al., 2001). The strain parameters solved by the displacement model represent the deformation at each point on the object. Assuming that the deformation varies continuously from one point to another, the strain field can be estimated. In contrast, the strain parameters solved by the affine model represent deformation in each study area of the object and therefore lead to discontinuity between any two different study areas. In practice, strain fields are barely homogeneous due to the non-uniformity of materials; for this reason, the displacement model is more suitable for practical use.

Considering the displacement of an initial point as a constant vector, the mathematical model can be solved easily by an ordinary indirect observations approach. For cases involving a large number of observations, nevertheless, the displacement of the initial point is more likely to be an observation. Therefore, the unified least-squares approach is adopted in this study. By changing the weight of parameter observations, the accuracy of the displacement of the initial point can be evaluated properly in the model. After evaluating each parameter in the model, the quality of every parameter is also assessed based on the law of error propagation. Moreover, sensitivity analysis (Koch, 1988; Han et al., 2011) is introduced to estimate the minimum deformation that can be detected by the network. Finally, two strategies are built for analyzing a vast number of spatial data. Ultimately, a complete deformation analysis procedure is established. With a large number of observations like DIC or LiDAR datasets, the proposed method determines the strain field of an object, as well as the quality and sensitivity of the parameters.

METHODOLOGY

Strain field determination

Choosing an arbitrary point on an object as the starting point, the deformation at that point can be expressed by the coordinates and displacement measurements of the starting point and its several neighboring points:

$$\mathbf{u}_j = \mathbf{H}_i \cdot \Delta\mathbf{x}_{ij} + \mathbf{u}_i \tag{1}$$

Where $\mathbf{u}_i$ is the displacement vector of the starting point, $\mathbf{u}_j$ is the displacement vector of neighboring points, $\Delta\mathbf{x}_{ij}$ is the coordinate differences between the starting point and its neighboring points, and $\mathbf{H}_i$ is the displacement gradient tensor of the starting point. Rewriting Equation 1 in matrix form, we get:

$$\begin{bmatrix} u_{xj} \\ u_{yj} \\ u_{zj} \end{bmatrix} = \begin{bmatrix} h_{11} & h_{12} & h_{13} \\ h_{21} & h_{22} & h_{23} \\ h_{31} & h_{32} & h_{33} \end{bmatrix} \begin{bmatrix} \Delta x \\ \Delta y \\ \Delta z \end{bmatrix} + \begin{bmatrix} u_{xi} \\ u_{yi} \\ u_{zi} \end{bmatrix} \tag{2}$$

In this study, the unified least-squares approach (Mikhail et al., 2001) is used to properly provide uncertainty estimation for the displacement vector of the starting point and to better evaluate the unknown parameters in the model. The general form of the unified least-squares approach can be written as:

$$\mathbf{A}\mathbf{v} + \mathbf{B}\Delta = \mathbf{f} \tag{3}$$

$$\mathbf{v}_x - \Delta = \mathbf{f}_x = \mathbf{l}_x^0 - \mathbf{l}_x \tag{4}$$

Where Δ is the unknown parameter, $\mathbf{l}_x$ is the parameter observation, $\mathbf{l}_x^0$ is the parameter approximation, $\mathbf{v}$ and $\mathbf{v}_x$ are residuals, $\mathbf{A}$ and $\mathbf{B}$ are coefficient matrices, and $\mathbf{f}$ and $\mathbf{f}_x$ are constant vectors.

By considering the displacement vector of the starting point ($\mathbf{u}_i$) as the parameter observation, the displacement vector of neighboring points ($\mathbf{u}_j$) as observations, coordinate differences ($\Delta\mathbf{x}_{ij}$) as constants, and the displacement gradient matrix ($\mathbf{H}_i$) as unknown, the displacement model (Equation 1) can be rewritten in least-squares form, forming matrices $\mathbf{A}$, $\mathbf{B}$, and $\mathbf{f}$:

$$\mathbf{v} + \begin{bmatrix} -\Delta x_{i1} & -\Delta y_{i1} & -\Delta z_{i1} & 0 & 0 & 0 & 0 & 0 & 0 & -1 & 0 & 0 \\ 0 & 0 & 0 & -\Delta x_{i1} & -\Delta y_{i1} & -\Delta z_{i1} & 0 & 0 & 0 & 0 & -1 & 0 \\ 0 & 0 & 0 & 0 & 0 & 0 & -\Delta x_{i1} & -\Delta y_{i1} & -\Delta z_{i1} & 0 & 0 & -1 \\ \vdots & \vdots & \vdots & \vdots & \vdots & \vdots & \vdots & \vdots & \vdots & \vdots & \vdots & \vdots \\ -\Delta x_{in} & -\Delta y_{in} & -\Delta z_{in} & 0 & 0 & 0 & 0 & 0 & 0 & -1 & 0 & 0 \\ 0 & 0 & 0 & -\Delta x_{in} & -\Delta y_{in} & -\Delta z_{in} & 0 & 0 & 0 & 0 & -1 & 0 \\ 0 & 0 & 0 & 0 & 0 & 0 & -\Delta x_{in} & -\Delta y_{in} & -\Delta z_{in} & 0 & 0 & -1 \end{bmatrix} \begin{bmatrix} h_{11} \\ h_{12} \\ h_{13} \\ h_{21} \\ h_{22} \\ h_{23} \\ h_{31} \\ h_{32} \\ h_{33} \\ u_{xi} \\ u_{yi} \\ u_{zi} \end{bmatrix} \tag{5}$$

$$= \begin{bmatrix} -u_{x1} & -u_{y1} & -u_{z1} & \cdots & -u_{xn} & -u_{yn} & -u_{zn} \end{bmatrix}^T$$

Besides forming all the matrices needed, the values and weights of parameter observations must be given. For the parameter observations related to the displacement gradient matrix, the values are assumed to be zero since no information about the deformation parameters is provided. For the other parameter observations related to the displacement vector of the starting point, the values are set to be the displacement measurements at the starting point. Note that the governing equations are linear, which means no iteration will be needed in the computation, and therefore the $\mathbf{l}_x^0$ in Equation 4 is a zero vector. According to the above, we can form the matrix $\mathbf{f}_x$:

$$\mathbf{f}_x = \mathbf{l}_x^0 - \mathbf{l}_x = \begin{bmatrix} 0 & 0 & 0 & 0 & 0 & 0 & 0 & 0 & 0 & -u_{xi} & -u_{yi} & -u_{zi} \end{bmatrix}^T \tag{6}$$

The weight of the parameter observations can be divided into two parts:

$$\mathbf{W}_{xx} = \begin{bmatrix} \mathbf{W}_a & \mathbf{0} \\ \mathbf{0} & \mathbf{W}_b \end{bmatrix} \tag{7}$$

Where $\mathbf{W}_a$ represents the weight of parameter observations and $\mathbf{W}_b$ represents the weight of the displacement vector of the starting point. Setting $\mathbf{W}_a \cong 0$, since there is no information about strain parameters, the value of $\mathbf{W}_b$ is given according to the accuracy of the observation. Ultimately, applying the least-squares principle, we get:

$$\mathbf{N} = \mathbf{B}^T \mathbf{W} \mathbf{B} \tag{8}$$

$$\mathbf{t} = \mathbf{B}^T \mathbf{W} \mathbf{f} \tag{9}$$

$$\boldsymbol{\Delta} = (\mathbf{N} + \mathbf{W}_{xx})^{-1} (\mathbf{t} - \mathbf{W}_{xx} \mathbf{f}_x) \tag{10}$$

Where **W** is the weight of observations. Once the least-squares problem is solved, the displacement gradient matrix $\mathbf{H}_i$ is obtained, and the strain tensor of the starting point can be computed:

$$\boldsymbol{\varepsilon}_i = \frac{1}{2}(\mathbf{H} + \mathbf{H}^T + \mathbf{H}^T \mathbf{H}) \approx \frac{1}{2}(\mathbf{H}_i + \mathbf{H}_i^T) \tag{11}$$

Note that the high-order terms can be ignored under the assumption of small deformation, and therefore the strain tensor $\boldsymbol{\varepsilon}_i$ is symmetric. By applying singular value decomposition, the strain tensor can be decomposed into two components: a diagonal matrix $\boldsymbol{\Lambda}$ and an orthogonal matrix $\mathbf{S}$:

$$\boldsymbol{\varepsilon}_i = \mathbf{S}^T \boldsymbol{\Lambda} \mathbf{S} \tag{12}$$

Where the diagonal entries of matrix $\boldsymbol{\Lambda}$ represent three principal strains respectively, and the corresponding principal directions are defined by the columns of matrix $\mathbf{S}$.

Using the unified least-squares technique, the displacement of the starting point can be considered as a constant, observation, or unknown by simply giving different weights without changing the equation, making the displacement model more feasible for various situations. For every point (with displacement observation) in a given network, the displacement can be considered as an observation properly. Moreover, for points without displacement observation, the deformation can be estimated by assuming the displacement observation to be unknown. Consequently, deformation of any given point in the study area can be solved by the proposed method.

Quality assessment

The cofactor matrices of the unknown parameter, strain tensor, and principal strain can be propagated one by one according to the law of propagation. Starting with the cofactor matrix of observation **Q** and the cofactor matrix of parameter observation $\mathbf{Q}_{xx}$, the cofactor matrix of unknown parameters can be obtained:

$$\mathbf{Q}_{\Delta\Delta} = (\mathbf{B}^T \mathbf{W} \mathbf{B} + \mathbf{W}_{xx})^{-1} \tag{13}$$

Selecting all the elements related to the displacement gradient matrix $\mathbf{H}_i$ in $\mathbf{Q}_{\Delta\Delta}$, we get the cofactor matrix of the displacement gradient matrix ($\mathbf{Q}_\mathbf{H}$). Then, the cofactor matrix of the strain tensor can be computed based on Equation 11:

$$\mathbf{Q}_\varepsilon = \mathbf{D}_\mathbf{H} \mathbf{Q}_\mathbf{H} \mathbf{D}_\mathbf{H}^T \tag{14}$$

Where $\mathbf{D}_\mathbf{H}$ is a coefficient matrix,

$$\mathbf{D}_\mathbf{H} = \begin{bmatrix} 1 & 0 & 0 & 0 & 0 & 0 & 0 & 0 & 0 \\ 0 & 0 & 0 & 0 & 1 & 0 & 0 & 0 & 0 \\ 0 & 0 & 0 & 0 & 0 & 0 & 0 & 0 & 1 \\ 0 & 0.5 & 0 & 0.5 & 0 & 0 & 0 & 0 & 0 \\ 0 & 0 & 0.5 & 0 & 0 & 0 & 0.5 & 0 & 0 \\ 0 & 0 & 0 & 0 & 0 & 0.5 & 0 & 0.5 & 0 \end{bmatrix} \tag{15}$$

To get the cofactor matrix of principal components, listing all the elements in matrix $\boldsymbol{\Lambda}$ and $\mathbf{S}$ firstly:

$$\boldsymbol{\lambda} = \begin{bmatrix} \lambda_1 & \lambda_2 & \lambda_3 \end{bmatrix}^T \tag{16}$$

$$\text{vec}(\mathbf{S}) = \begin{bmatrix} s_{11} & s_{21} & s_{31} & s_{12} & s_{22} & s_{32} & s_{13} & s_{23} & s_{33} \end{bmatrix}^T \tag{17}$$

According to Han et al. (2007), the cofactor matrix of principal components $\mathbf{Q}_{\{\lambda, \text{vec}(\mathbf{S})\}}$ can be derived by:

$$\mathbf{Q}_{\{\lambda, \text{vec}(\mathbf{S})\}} = \mathbf{K} \mathbf{Q}_\varepsilon \mathbf{K}^T \tag{18}$$

$$\mathbf{K} = \begin{bmatrix} \mathbf{I} & \mathbf{0} \\ \mathbf{0} & -(\mathbf{I} \otimes \mathbf{S}) \mathbf{D}_\Omega \end{bmatrix} \tilde{\mathbf{F}}^{-1} \tag{19}$$

$$\tilde{\mathbf{F}} = \mathbf{D}_E \left(\mathbf{S}^T \square \mathbf{S}^T \quad \vdots \quad -\left(\mathbf{D}_S + \mathbf{I}\right)\left(\mathbf{I} \otimes \boldsymbol{\varepsilon}\right)\mathbf{D}_\Omega \right) \qquad (20)$$

Where the operator $\otimes$ denotes the Kronecker product, the operator $\square$ denotes the Khatri-Rao product, and $\mathbf{D}_E$, $\mathbf{D}_S$, and $\mathbf{D}_\Omega$ are coefficient matrices. Once the cofactor matrices $\mathbf{Q}_{\Delta\Delta}$, $\mathbf{Q}_\varepsilon$, and $\mathbf{Q}_{\{\lambda, \text{vec}(\mathbf{S})\}}$ have been derived, the quality of deformation parameters of the proposed method can be evaluated on a solid basis.

Sensitivity analysis

Sensitivity analysis was applied to estimate minimum detectable deformation signals under a given network and statistical distribution. Han et al. (2011) introduced this technique to principal strain parameters and derived the significant critical variation value:

$$\left\| \Delta \right\|_i = \frac{\delta_0 \sigma_0}{\sqrt{\lambda'_{\Delta_i}}} \qquad (21)$$

Where σ_0^2 is the variance of unit weight, δ_0 is the non-centrality parameter of a normal distribution expressed by a significant level α and a test power β, λ'_{Δ_i} is the ith eigenvalue of $\mathbf{Q}_\Delta^{-1}$, and $\mathbf{Q}_\Delta$ is the cofactor matrix of principal strain parameters.

The critical value denotes the minimum deformation which can be detected under a given network. The smaller the value, the better the capability of detecting variations, which implies a higher sensitivity. The critical value of principal strain can be calculated by substituting the corresponding entry of the cofactor matrix of principal strain parameters, $\mathbf{Q}_{\{\lambda, \text{vec}(\mathbf{S})\}}$, into Equation 21.

Comparing the critical value with the strain parameter, whether the parameters have shown significant differences is determined immediately. Given the accuracy of observations, sensitivity analysis provides a method of estimating the significance of deformation. Equally importantly, if the object is partially changed, the deformed area will be distinguished.

Strategies for analyzing a large number of data

Since the displacement vectors in the mathematical model are related to displacement of the starting point ($\mathbf{u}_i$) and its neighboring points ($\mathbf{u}_j$), the first step of deformation analysis is to specify the study area, namely, to choose the neighboring points corresponding to each starting point. When introducing a large number of points to the analysis, the study area should be limited to several points close to the starting point, because: (1) distant points have a minor effect on the deformation of the starting point, and (2) too many data will cause low efficiency in computation. In this study, two strategies are used to specify the neighboring region for each starting point: Nearest Neighbor Search (NNS) and Triangulated Irregular Network (TIN).

The nearest neighbor search identifies the top k nearest neighbors to the starting point as neighboring points. In a 3D deformation analysis, k should be more than or equal to four in order to provide a sufficient number of equations and solve the

unknown parameters. A larger k means more neighboring points will be involved when determining the strain of the starting point. While adding new points may reduce the residuals in the least-squares approach, involving too many distant points will only blur the pattern of strain field. To choose an optimal k, one can start from the minimum, and gradually increase k until the quality of least-squares solution meets the requirements. Furthermore, the network configuration corresponding to each starting point will not be the same because the nearest neighbor search operates independently each time. Since the algorithm chooses neighboring points blindly without considering the network configuration, it is more suitable for uniform data.

The simplest solution for the NNS problem is to calculate the distance from the starting point to every other point in the network (the "brute-force solution"). However, the algorithm has a poor performance, that is, a running time of $O(n^d)$, where n is the number of points in the network and d is the dimension of space. In this study, the spatial index method is used to improve the performance of NNS. A rectangular grid is created first, and then every point in the network is allocated to its relevant position in the grid. For any starting point i in a grid cell, the search region will be reduced to points in the cell and in its adjacent cells (Figure 1). The spatial index method yields the same result as the brute-force solution but with higher performance, especially when the points are uniformly distributed in space.

Another method of identifying the study area is TIN. Creating a TIN specifies a neighboring region for each starting point immediately: the neighboring points comprise every point that shares an edge with the starting point. For every starting point, the study area is a proportion of the entire triangulation, and so the complete network configuration remains the same. The number of neighboring points for each starting point will be different. For points lying on the edge of a network, the number of neighboring points is often insufficient; that is, there are fewer equations than unknowns in the linear system. In this case, a method that integrates NNS with TIN is applied: if the first connection cannot provide enough neighboring points, the top m nearest points in the second connection will be added as new neighbors in order to solve the linear system.

Summing up, both NNS and TIN can specify the neighboring region corresponding to each starting point efficiently. While NNS has higher performance, TIN builds a fixed network. In practice, NNS is more suitable for a uniformly distributed dense dataset; as for a sparse dataset, using TIN to generate a fixed network configuration is better.

RESULTS AND DISCUSSION

Efficiency of 3D dispersed data analysis

The efficiency of applying the NNS brute-force solution, the NNS spatial index solution, and TIN on a LiDAR dataset was tested in this experiment. The dataset contained a total of 360330 dispersed points. To test the efficiency of different search methods, we applied systematic sampling on the LiDAR dataset with different sampling intervals, and get six subsets containing 5000, 10000, 15000, 20000, 25000, and 30000 points respectively. Four search methods (Table 1) were used to find the neighboring points corresponding to each point in the subsets. The algorithms were implemented using MATLAB (R2013a, 64-bit), and the hardware used to test the running time is shown in Table 2. The running times
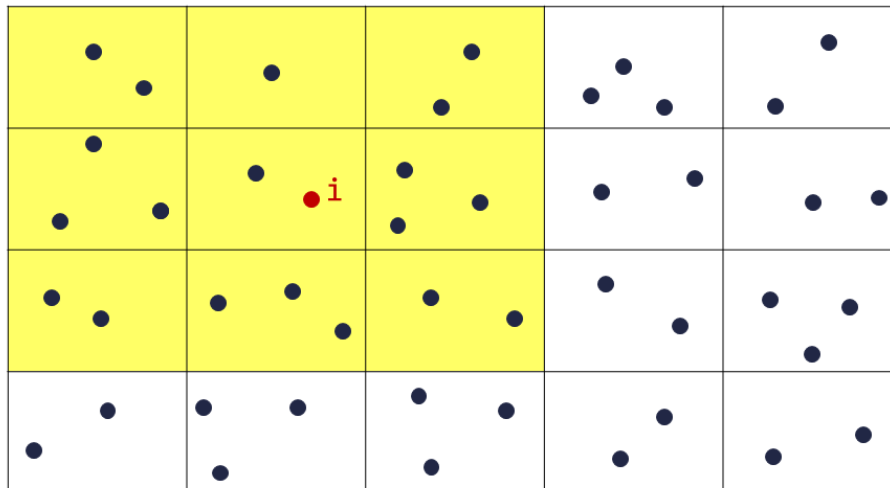
Figure 1. Search region for point *i* using the spatial index method.

Table 1. Four different search strategies for specifying the neighboring region.

Method	Definition of neighboring region	Strategy
1	Top four nearest points	Brute-force solution
2	Top four nearest points	Spatial index method with $5\times1\times5$ grid
3	Top four nearest points	Spatial index method with $20\times1\times20$ grid
4	TIN (At least four points)	TIN (and NNS if the number of points is less than four in the first connection)

Table 2. Hardware used in the running time test.

Model	Toshiba Satellite M840
Processor	Intel Core i5-3210M 2.5/3.1GHz
Memory	8G DDR3 1600MHz
Operating system	Microsoft Windows 7 Home Premium 64bit

for each search method are shown in Figure 2. When applying the NNS solution, the result showed that even a coarse grid could reduce the running time significantly. As the number of points increased, the difference between the brute-force solution and the spatial index method became considerable. In the case in which the number of points is 30000, the brute-force solution (method 1) took about 98 s to find the neighboring points, while method 2 took 27 s and method 3 took only 4 s, providing time savings of 72 and 96% respectively. Figure 2 also shows that the running time of the TIN solution was shorter than that of the NNS brute-force solution but longer than that of the NNS $20\times1\times20$ gridded solution, which indicates that the performance will still be poor when the number of points grows larger. As a consequence, the NNS solution with a proper grid is the best choice when taking performance into consideration.

Bending test with real data

A bending test and a close-range photogrammetry survey were carried out. The sample was fixed on the testing machine and subjected to an external load that increased at a constant rate until fracture occurred. At the same time, the in-plane displacement fields on the sample's surface at each epoch were acquired by the photogrammetry technique. The strain fields were calculated based on the proposed method and the observed displacement fields; in addition, the quality and sensitivity of strain parameters were also evaluated.
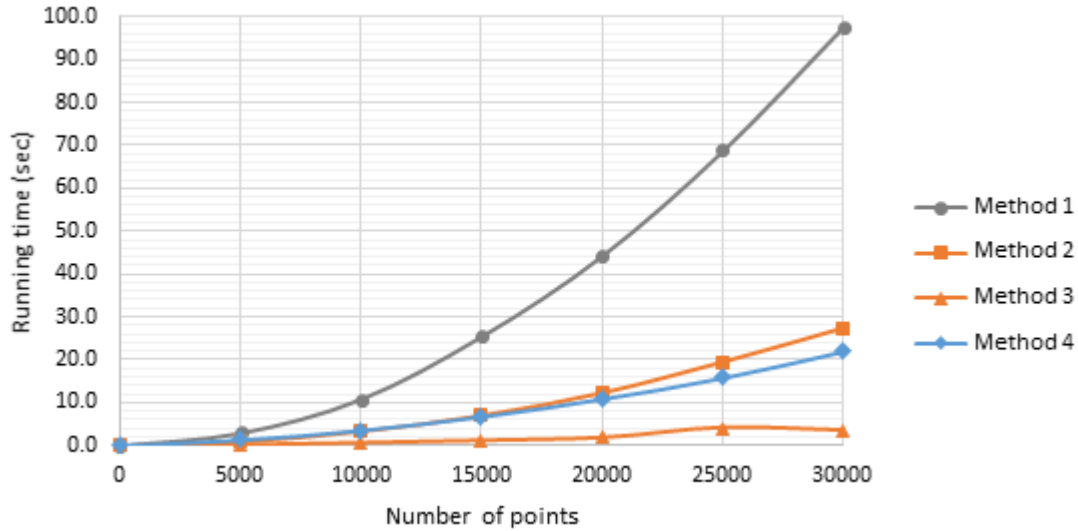
Figure 2. Running time for each method.

The sample used in the bending test was a $340\,\mathrm{mm} \times 50\,\mathrm{mm}$ aluminum specimen. The specimen was painted with a coating of coarse particles on one side for template matching, and three sets of KYOWA strain gauges (Model: KFG-1-120-D17-11L3M2S; accuracy: approximately 0.1%) were pasted on the other side. The displacement-controlled method was conducted, applying a displacement increment and taking an image of the specimen every 3 s. Before the fracture occurred, displacement fields at 81 different epochs were collected, where epoch 1 was the reference epoch (that is, without external load), and the specimen failed at epoch 81.

A close-range photogrammetric survey was conducted using two digital cameras (Canon EOS 550D). The cameras were fixed on tripods during the whole experiment, and the object distance was approximately 1 m. The digital image correlation (DIC) technique of template matching, implemented with OpenCV library, was used to calculate the coordinates of every point on the specimen at each epoch. Taking epoch 1 as the reference epoch, the displacement fields at the other 80 epochs were obtained immediately. The overall accuracy was approximately $10^{-5}\,\mathrm{m}$ since the result of camera calibration was 0.2 to 0.4 pixels and 1 pixel in the image space was equal to 0.05 mm in the object space.

Strain field determination

The strain field on the sample's surface was determined by the displacement gradient model and unified least-squares technique using the point coordinates and displacement field obtained by the DIC technique. The NNS spatial index solution was adopted to choose the nearest eight points as neighboring points. The strain parameters were solved with an accuracy of ± 0.0014. The obtained λ_1 and λ_2 strain fields at different epochs are shown in Figures 3 and 4, respectively. Since the specimen failed at epoch 81, by comparing the pattern of fracture shown in Figure 5 and the strain field at epoch 80 (plot with a different scale in Figure 6 to clearly illustrate where the maximum strain happened), one can immediately find that the specimen broke where the maximum strain happened. The result shows one main difference between strain field determination and the strain gauges' measurements: the former solves the complete strain field and can thus detect the position at which the fracture occurs; the latter only measures strain where the gauges are installed. In conclusion, the proposed method can determine the strain field, showing the differences between epochs; thus, it is able to detect the position in which maximum strain happens, which is where the fracture may occur.

Statistical significance

The main goal of sensitivity analysis is to estimate the capability of detecting deformations of a network. Based on the result of quality assessment and setting the significance level $\alpha = 0.05$ and the test power $\beta = 0.95$, the significant critical variation values corresponding to every point in the network were calculated. Whether the deformation at a point was detectable could be distinguished by comparing its critical value to the strain parameter. The red areas in Figure 7 show the significant deformed areas on the specimen at different epochs.
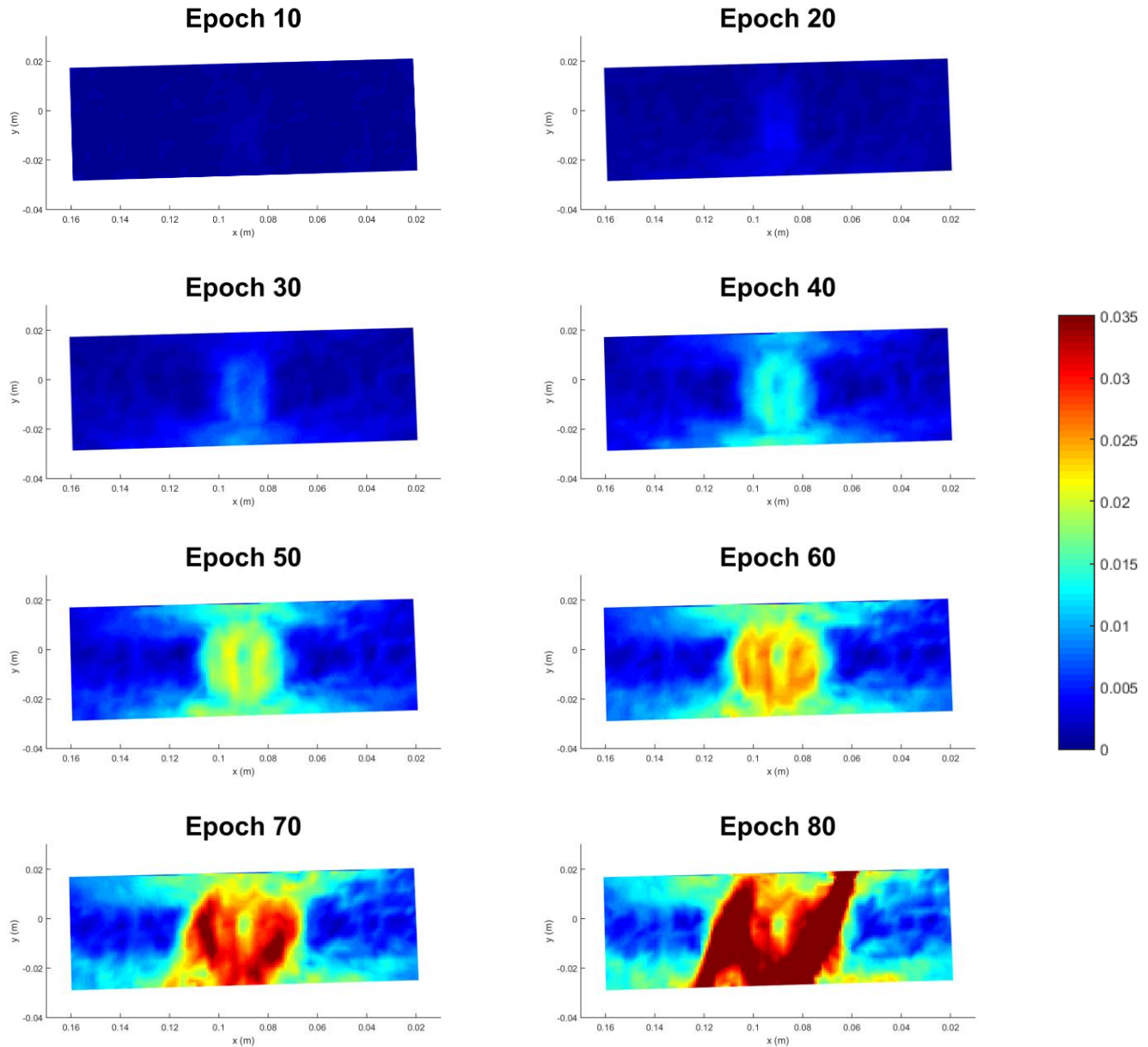
Figure 3. The λ_1 strain field at eight different epochs.

The significance of deformation parameters is affected by the accuracy of observation and the strength of the network. The critical value decreases with increased accuracy and strength of the network, implying better capability of detecting deformation. In this experiment, the average critical value is 0.0046, which means the minimum deformation that can be detected is about 0.46%. The critical value provides a method of determining whether or where the statistical significant deformation happens. For this reason, it is especially important in early epochs, that is, when the deformations are small.

CONCLUSION

In this study, the displacement model is chosen to estimate nonhomogeneous deformation, and the unified least-squares adjustment is used to assess the accuracy of deformation parameters properly. By giving different weights, the characteristics of parameters can be altered easily, making the displacement model more feasible for various circumstances. Also, the accuracy and the significant critical value of strain parameters are derived, providing a reliable quality assessment and effectively
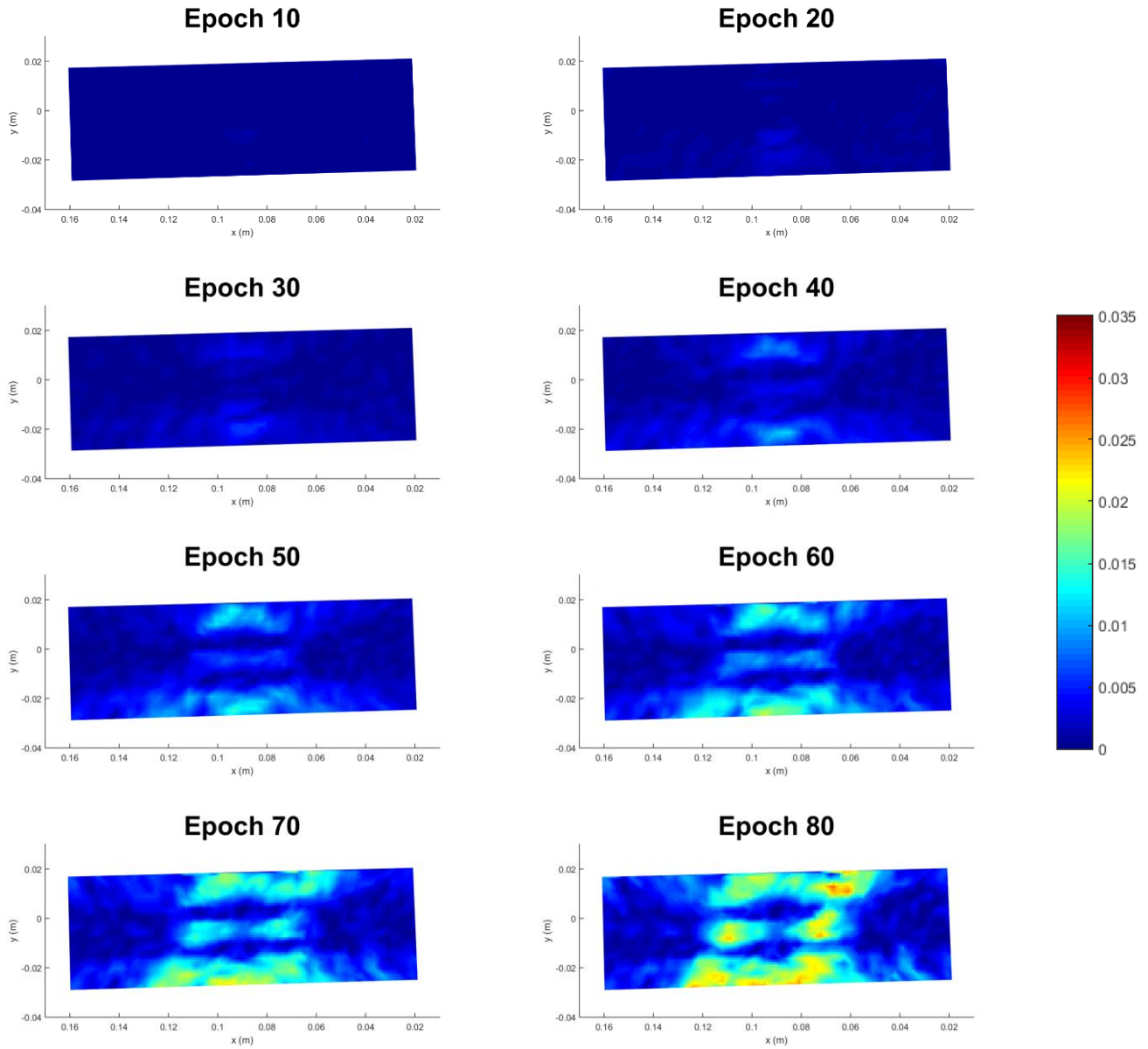
Epoch 10

Epoch 20

Epoch 30

Epoch 40

Epoch 50

Epoch 60

Epoch 70

Epoch 80

Figure 4. The λ_2 strain field at eight different epochs.

Figure 5. Pattern of fracture.

detecting the significant deformed area. For analyzing numerous point data, the nearest neighbor search and triangulated irregular network are introduced to specify the neighboring points, and the spatial index method is
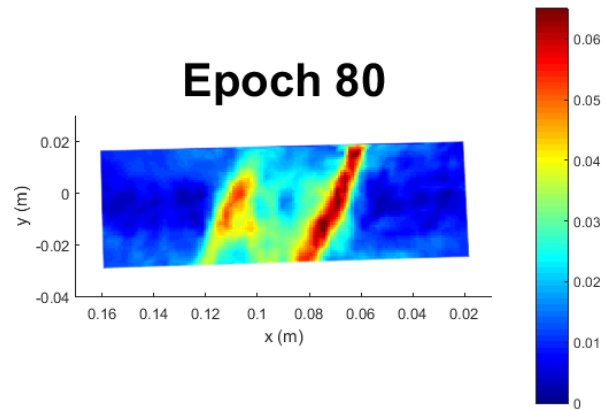
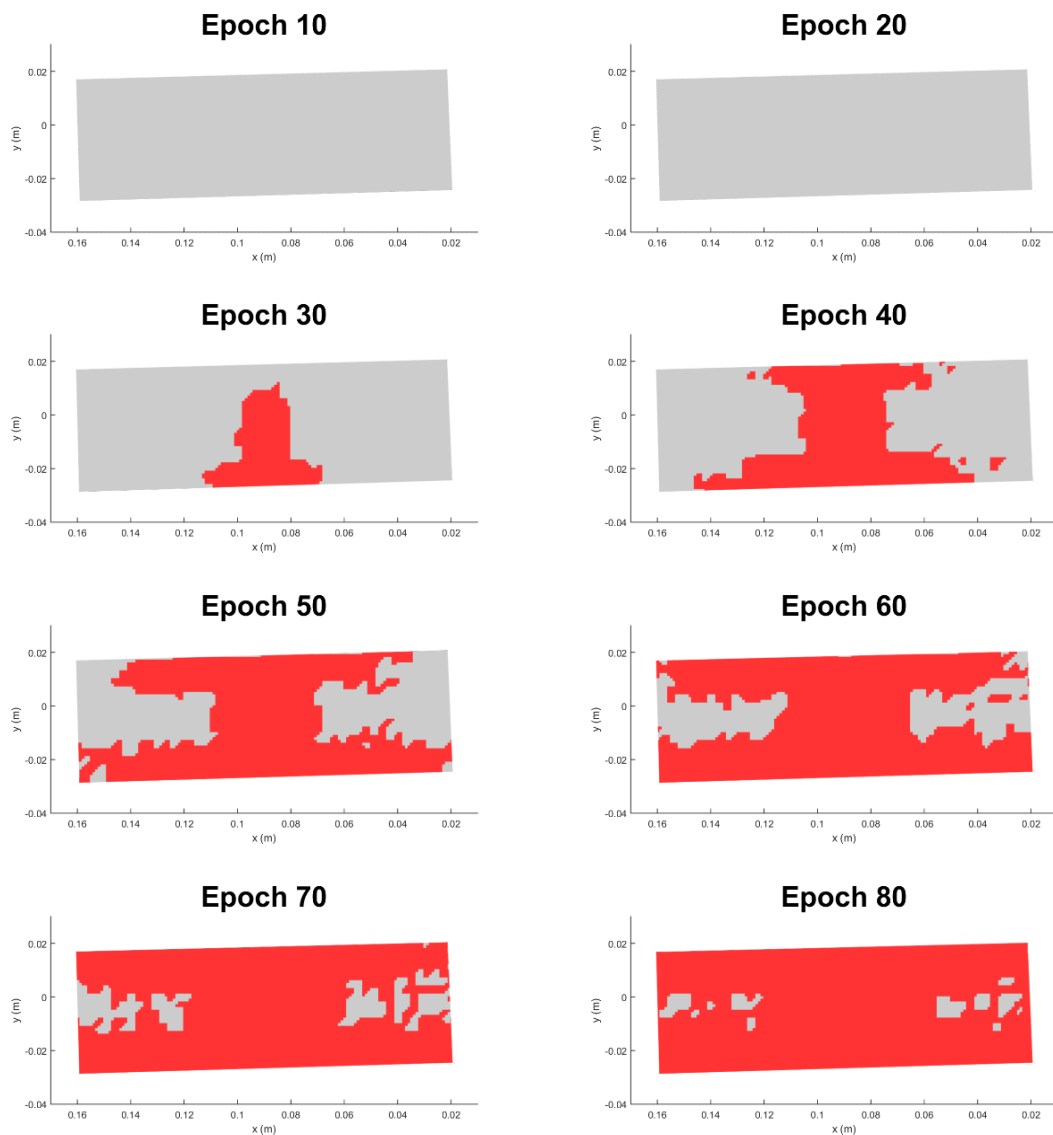**Figure 6.** λ_1 strain field at epoch 80.

Figure 7. The significant deformed area (red area) on the specimen at eight different epochs.

adopted to reduce the running time. Numerical experiments showed that the variation as well as the extreme value of the strain field can be detected efficiently. Summing up, the strain field on the surface of an object can be obtained rapidly and accurately by applying the proposed method to a large number of spatial data.

Conflict of Interests

The authors have not declared any conflict of interests.

ACKNOWLEDGMENTS

REFERENCES

Alba M, Scaioni M (2010). Automatic detection of changes and deformation in rock faces by terrestrial laser scanning. In *Proc.* ISPRS Commission 1501:11-16.

Armesto J, Roca-Pardiñas J, Lorenzo H, Arias P (2010). Modelling masonry arches shape using terrestrial laser scanning data and nonparametric methods. Eng. Struct. 32(2):607-615.

Aydilek AH, Guler M, Edil TB (2004). Use of image analysis in determination of strain distribution during geosynthetic tensile testing. J. Comput. Civil. Eng. 18(1):65-74.

Berber M, Dare P, Vaníček P (2006). Robustness analysis of two-dimensional networks. J. Surv. Eng. - ASCE. 132(4):168-175.

Chu TC, Ranson WF, Sutton MA (1985). Applications of digital-image-correlation techniques to experimental mechanics. Exp. Mech. 25(3):232-244.

González-Jorge H, Riveiro B, Armesto J, Arias P (2011). Verification artifact for photogrammetric measurement systems. Opt. Eng. 50(7):073603-073603.

Gonzalez-Jorge H, Riveiro B, Armesto J, Arias P (2012). Procedure to evaluate the accuracy of laser-scanning systems using a linear precision electro-mechanical actuator. IET. Sci. Meas. Technol. 6(1):6-12.

Han JY, Guo J, Zheng ZY (2011). Sensitivity analysis for the principal strain parameters of a deformation monitoring network. J. Surv. Eng. ASCE. 138(3):109-116.

Han JY, Van Gelder BHW, Soler T (2007). On covariance propagation of eigenparameters of symmetric nD tensors. Geophys. J. Int. 170(2):503-510.

Han JY, Van Gelder BHW, Lin SL (2009). Rotation- and translation-free estimations of symmetric, rank-two tensors with a case study in LIDAR surveying. J. Surv. Eng. ASCE. 136(1):23-28.

Koch KR (1988). Bayesian statistics for variance components with informative and noninformative priors. Manuscr. Geodaet. 13:370-373.

Lee HM, Park HS (2011). Gage-free stress estimation of a beam-like structure based on terrestrial laser scanning. Comput.-Aided. Civ. Inf. 26(8):647-658.

Lee C, Take WA, Hoult NA (2011). Optimum accuracy of two-dimensional strain measurements using digital image correlation. J. Comput. Civil. Eng. 26(6):795-803.

Marjetič A, Ambrožič T, Turk G, Sterle O, Stopar B (2009). Statistical

properties of strain and rotation tensors in geodetic network. J. Surv. Eng. ASCE. 136(3):102-110.

Mikhail EM, Bethel JS, McGlone JC (2001). Introduction to Modern Photogrammetry, John Wiley & Sons.

Pan B, Qian K, Xie H, Asundi A (2009). Two-dimensional digital image correlation for in-plane displacement and strain measurement: A review. Meas. Sci. Technol. 20(6):062001.

Pan B, Yuan J, Xia Y. (2015). Strain field denoising for digital image correlation using a regularized cost-function. Opt. Laser. Eng. 65:9-17.

Park HS, Lee HM, Adeli H, Lee I (2007). A new approach for health monitoring of structures: terrestrial laser scanning. Comput.-Aided. Civ. Inf. 22(1):19-30.

Pesci A, Casula G, Boschi E (2011). Laser scanning the Garisenda and Asinelli towers in Bologna (Italy): detailed deformation patterns of two ancient leaning buildings. J. Cult. Herit. 12(2):117-127.

Vaníček P, Craymer MR, Krakiwsky EJ. (2001). Robustness analysis of geodetic horizontal networks. J. Geodesy 75(4):199-209.

Vaníček P, Grafarend EW, Berber M. (2008). Short note: Strain invariants. J. Geodesy 82(4/5):263-268.

Winkler J, Fischer G, Georgakis CT (2014). Measurement of local deformations in steel monostrands using digital image correlation. J. Bridge Eng. 19(10):04014042.

Scientific Research and
Essays

Related Journals Published by Academic Journals

- African Journal of Mathematics and Computer Science Research
- International Journal of Physical Sciences
- Journal of Oceanography and Marine Science
- International Journal of Peace and Development Studies
- International NGO Journal